# A CMOS Multi-Modal Electrochemical and Impedance Cellular Sensing Array for Massively Paralleled Exoelectrogen Screening

Sagar R. Kumashi , Student Member, IEEE, Doohwan Jung, Student Member, IEEE,
Jongseok Park , Member, IEEE, Sara Tejedor Sanz , Sandra Grijalva, Adam Wang , Student Member, IEEE,
Sensen Li , Student Member, IEEE, Hee Cheol Cho, Caroline M. Ajo-Franklin,
and Hua Wang , Senior Member, IEEE

Abstract—The paper presents a 256-pixel CMOS sensor array with in-pixel dual electrochemical and impedance detection modalities for rapid, multi-dimensional characterization of exoelectrogens. The CMOS IC has 16 parallel readout channels, allowing it to perform multiple measurements with a high throughput and enable the chip to handle different samples simultaneously. The chip contains a total of 2  $\times$  256 working electrodes of size 44  $\mu$ m  $\times$  52  $\mu$ m, along with 16 reference electrodes of dimensions 56  $\mu$ m imes 399  $\mu$ m and 32 counter electrodes of dimensions 399  $\mu$ m  $\times$  106  $\mu$ m, which together facilitate the high resolution screening of the test samples. The chip was fabricated in a standard 130nm BiCMOS process. The on-chip electrodes are subjected to additional fabrication processes, including a critical Al-etch step that ensures the excellent biocompatibility and long-term reliability of the CMOS sensor array in bio-environment. The electrochemical sensing modality is verified by detecting the electroactive analyte NaFeEDTA and the exoelectrogenic Shewanella oneidensis MR-1 bacteria, illustrating the chip's ability to quantify the generated electrochemical current and distinguish between different analyte concentrations. The impedance measurements with the HEK-293 cancer cells cultured on-chip successfully capture the cell-to-surface adhesion information between the electrodes and the cancer cells. The reported CMOS sensor array outperforms the conventional discrete setups for exoelectrogen characterization in terms of spatial resolution and speed, which demonstrates the chip's potential to radically accelerate synthetic biology engineering.

Manuscript received November 9, 2020; revised January 27, 2021; accepted February 24, 2021. Date of publication March 24, 2021; date of current version May 26, 2021. This work was supported in part by the U.S. Office of Naval Research under Grants N00014-16-1-2534 and N00014-17-1-2457 as well as National Science Foundation under Grants 1454555 and 1610677. (Corresponding Author: Sagar R. Kumashi)

Sagar R. Kumashi, Doohwan Jung, Adam Wang, Sensen Li, and Hua Wang are with the Georgia Institute of Technology, School of Electrical and Computer Engineering, Atlanta, GA 30332 USA (e-mail: sagar.kumashi@gatech.edu; djung44@gatech.edu; adam.y.wang@gatech.edu; lisensen@gatech.edu; hua.wang@ece.gatech.edu).

Jongseok Park is with Intel, Hillsboro, OR 97124 USA (e-mail: jongseok.park@intel.com).

Sara Tejedor Sanz is with Lawrence Berkeley National Laboratory, Molecular Foundry, Berkeley, CA 94720 USA (e-mail: stejedorsanz@lbl.gov).

Sandra Grijalva and Hee Cheol Cho are with the Emory University, Department of Biomedical Engineering, Atlanta, GA 30322 USA (e-mail: sandra.gonzalez@emory.edu; heecheol.cho@emory.edu).

Caroline M. Ajo-Franklin is with the Rice University, Department of Bio-Sciences, Houston, TX 77005 USA (e-mail: cajo-franklin@rice.edu).

Color versions of one or more figures in this article are available at https://doi.org/10.1109/TBCAS.2021.3068710.

Digital Object Identifier 10.1109/TBCAS.2021.3068710

Index Terms—Exoelectrogen, electrochemical sensing, impedance detection, multi-modality, microbial.

### I. INTRODUCTION

ROELECTROGENS are a class of micro-organisms that can transfer electrons between intracellular components and extracellular entities using special metabolic pathways [1], [2]. The currents produced due to these processes are harnessed by bioelectrochemical systems [3] such as microbial fuel cells (MFCs) and microbial electrolysis cells (MECs) for a diverse range of industrial and defense applications like waste water treatment [4]–[6], chemical synthesis [7], [8], toxic chemical sensing [9], [10], bio-computation [11] and energy production [1], [2]. Due to the unique current-generating ability of exoelectrogens, there is a natural interest in pairing them with semiconductor-based technologies to create hybrid cell-sensor systems that are self-sufficient. Previous works in the area of hybrid biotic-abiotic sensors [12], [13] have demonstrated the capability of such platforms to perform novel tasks which are beyond the scope of entirely electronic or biological systems.

Despite their versatile applications and remarkable properties, the utility of natural exoelectrogens has been limited by their low electron transfer rates [2] as well as their inability to derive energy from complex energy sources [16], [17] (Fig. 1). To redress these shortcomings, researchers resort to leveraging recent synthetic biology tools and genetically engineering the exoelectrogens to enhance their electrogenic capabilities or endow them with new features desirable for certain target applications [18], [19]. Genetic modification of exoelectrogenic bacteria utilizes the Design-Build-Test-Learn (DBTL) 4-phase development cycle, which is a common iterative process used to develop cell strains containing desired properties. As illustrated in Fig. 2, the DBTL cycle involves the systematic generation and evaluation of microbial strains and the knowledge accumulated over multiple iterations of the DBTL cycle guides the development of the desired genetic variant [20], [21]. Existing synthetic biology technologies have made the generation of massive genetic libraries possible, e.g., with 108 genetic variants, in the 'Build' phase. Unfortunately the "Test" phase of the constructed genetic variants is not able to keep pace with the 'Build' step.

1932-4545 © 2021 IEEE. Personal use is permitted, but republication/redistribution requires IEEE permission. See https://www.ieee.org/publications/rights/index.html for more information.

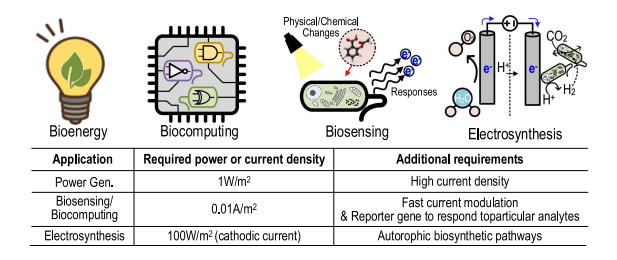


Fig. 1. Common applications of exoelectrogenic bacteria along with their requirements.

Presently, most labs still rely on bulky equipment and setups that can characterize only up to a few genetic species per day [15], [22], [23] (Fig. 2(a)). As a result, the 'Test' step imposes major restrictions on the overall efficacy of the DBTL cycle, and there is a need for screening technology platforms that can radically improve the throughput of exoelectrogen characterization orders of magnitude beyond the state of the art.

To completely characterize exoelectrogens, tracking markers of metabolic activity (e.g., electrochemical current, pH) in conjunction with various indicators of physical health and viability (e.g., Biofilm integrity) is crucial. As stated earlier, conventional exoelectrogen testing platforms, such as microbial fuel cells [15] and colorimetric detectors [24] suffer from low throughputs. This is attributed to their lack of compatibility with integrated electronics and poor scaling with small sample volumes. Popular electrochemical detection techniques such as voltammetry-based cell counting [25] offer improved speeds of characterization but are incapable of measuring the minute electrochemical currents originating from tiny volumes of exoelectrogens (typically 100fA/cell). While popular and standard cell cytometry techniques such as fluorescence activated cell sorting (FACS) [26] and impedance based Coulter counting [27] provide cellular resolution and can scan cells at high throughputs, their screening capabilities are intrinsically limited by fluorescent labels and their very short sensing windows (μs~ms). Hence they are incapable of capturing the slow electron transfer properties of exoelectrogenic species. In the same vein, more recent microelectronic approaches to cellular and molecular sensing [28]–[32] have been able to address the issues of throughput and sensitivity but they too provide information on only a single physical/chemical signal.

In summary, fully characterizing the genetic variants of exoelectrogens requires multi-modal sensing, while the complexity and long time-scales of electrochemical charge transfer [33] highlight the need for screening technologies that can support massive parallelism to match the throughput of genetic library generation.

To tackle these above-mentioned issues, we present a CMOS multi-sensor array [34] that can provide high throughput multi-parametric physiological information on a biological species of interest (Fig. 2(b)). The CMOS IC houses electrochemical detection modules that are composed of standard high-precision three-electrode potentiostats and high sensitivity current detection circuits to evaluate the current generating capacity of the exoelectrogens. The chip also hosts impedance sensing blocks that

measure cell adhesion to the chip surface and can track biofilm proliferation. The electrochemical and impedance sensing circuits share the usage of the  $\mu$ m-sized on-chip electrodes within each pixel. These electrodes undergo additional post-processing steps to enhance the electrochemical sensing performance and boost the biocompatibility of the chip. The improved robustness of the electrodes allows us to perform long duration experiments to track the slow metabolic activities of exoelectrogens. Furthermore, the small dimensions of the electrodes enable high resolution sensing of the test samples. The chip is divided into 16 pixel groups, with each one of them possessing their own electrodes and sensing circuits, making them capable of functioning autonomously. This ability can be fully leveraged by integrating the CMOS IC with droplet-based microfluidics, which will allow us to interrogate multiple samples simultaneously [35]. Moreover, the sample volume required for analysis in this case can be brought down to as low as 50nL, which is  $\sim 10^7$  times lower than the volume required by conventional exoelectrogen test setups [14], [15]. Hence, the large electrode array as well as the orthogonal sensing modalities present on chip can help us rapidly characterize multiple exoelectrogens and obtain a more holistic description of the tested micro-organisms, while utilizing much smaller sample volumes when compared to traditional reactor setups.

The subsequent sections are organized in the following manner: Section II describes the system architecture as well as the sensing circuitry. Section III elaborates on the post-processing protocols that were followed for the different on-chip electrodes. The results of the electrical characterization tests as well as the biological experiments are presented in Section IV.

## II. MULTI-MODAL ELECTROCHEMICAL AND IMPEDANCE SENSING ARRAY

The system architecture of the proposed joint electrochemical and impedance sensor array is displayed in Fig. 3. The chip contains 16 pixel-groups that share a global serial-to-parallel interface (SPI) block; which programs the various circuit blocks on chip; and a clock-generation module; which provides the excitation signal for impedance sensing.

Each pixel group has an array of  $4\times4$  sensing pixels, flanked by counter electrodes on the top and bottom as well as a reference electrode on the side. A single sensing pixel consists of two working electrodes that are reconfigured based on the active sensing modality. Each working electrode is  $44~\mu m \times 52~\mu m$  and the dimensions of the corresponding counter and reference electrodes are  $399~\mu m \times 106~\mu m$  and  $56~\mu m \times 399~\mu m$ , respectively. These electrode sizes were chosen after characterizing the current generating capacity of *Shewanella oneidensis* MR-1 bacteria with PCB electrodes. We arrived at the final electrode sizes after considering the current measured from the above mentioned experiments as well as the layout constraints imposed by the pixel circuitry.

The electrodes in each pixel group are accompanied by the corresponding excitation and sensing circuits for the inpixel dual sensing modalities. Both the electrochemical and impedance detection chains in a pixel group share a common

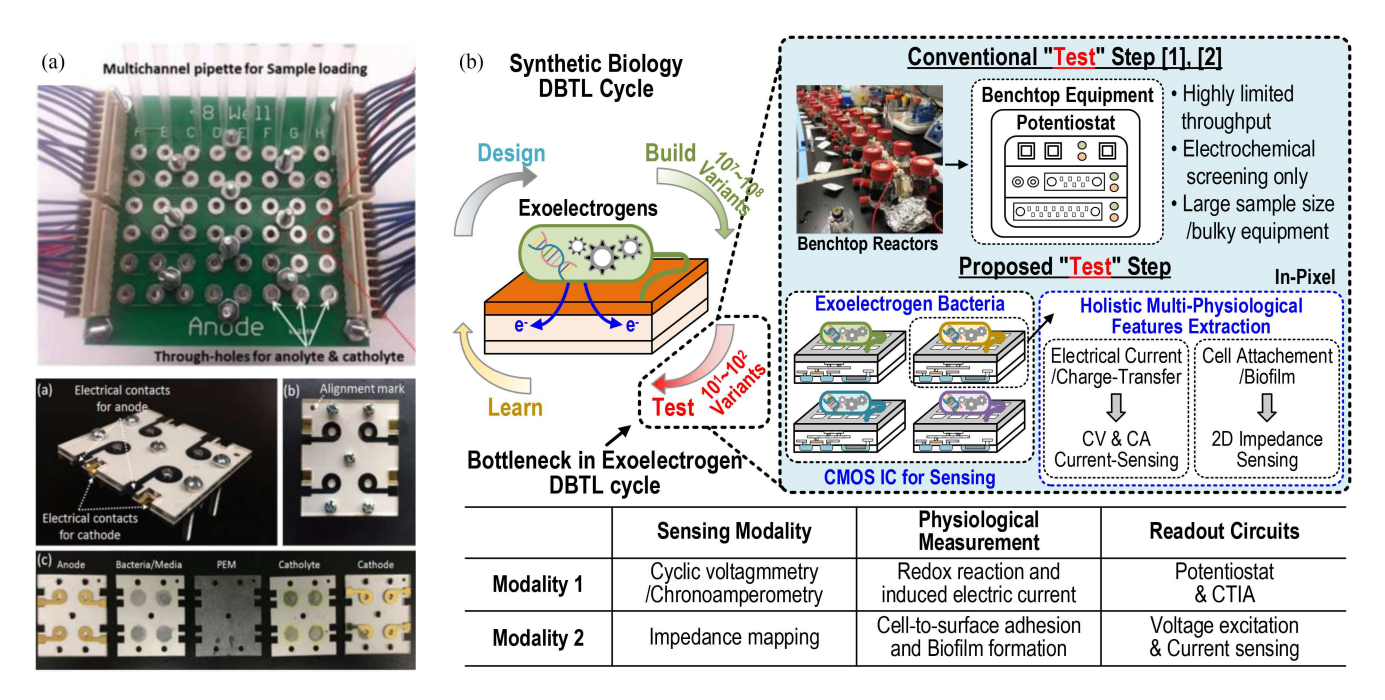


Fig. 2. (a) Examples of bulky testing setups used for exoelectrogen characterization [14], [15] (b) Conceptual Diagram depicting the DBTL cycle for exoelectrogens along with the shortcomings of traditional reactor-based test setups and the features of the reported CMOS platform.

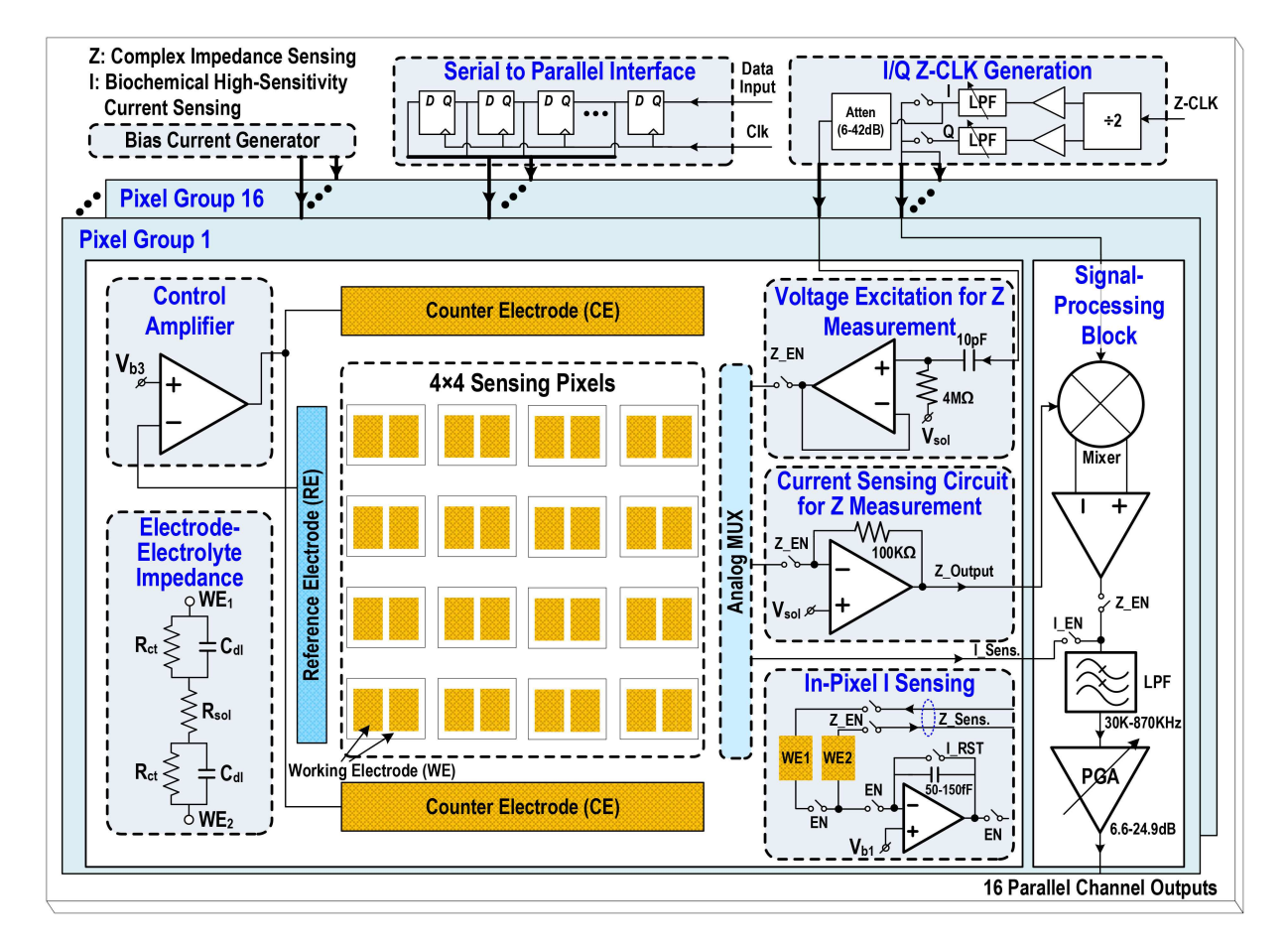


Fig. 3. Chip architecture of the joint electrochemical and impedance sensor array showing the various sensing circuit blocks and the electrode layout.

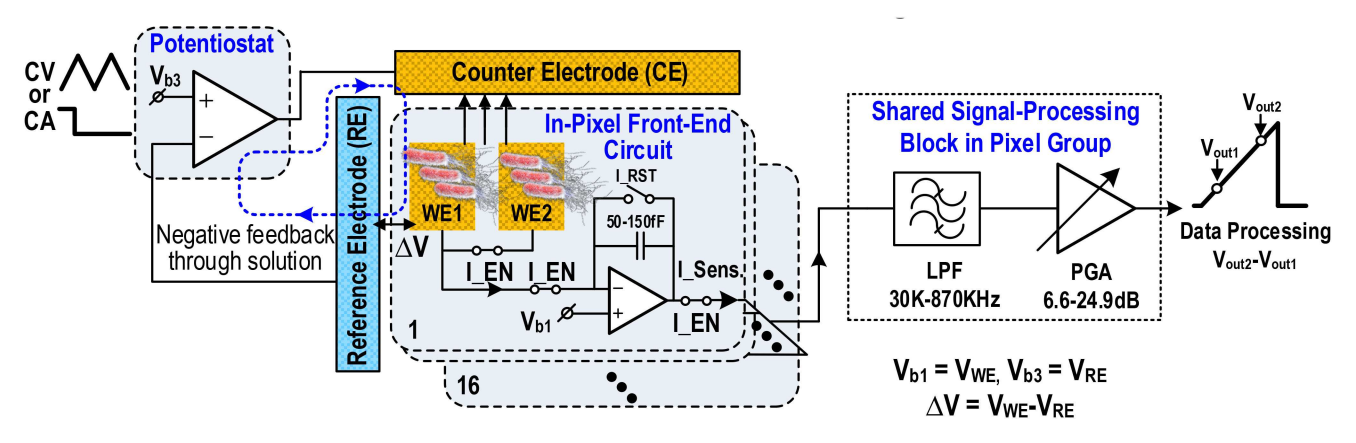


Fig. 4. Schematic of the on-chip potentiostat for high sensitivity electrochemical current sensing.

signal processing block that performs the required signal conditioning to ease the downstream analysis of the measured signals. Each signal processing block contains a mixer, for its complex impedance detection; a low pass filter (LPF) with a reconfigurable cut-off frequency (30KHz to 870kHz), to reject high frequency noise/image frequencies; and a programmable gain stage (6.6 to 24.9dB) at the end, to boost signal strength.

Hence, the entire chip houses  $2 \times 256$  working electrodes, 16 counter electrodes and 16 reference electrodes along with 16 electrochemical detection blocks and 16 impedance sensing blocks. In addition, the chip features 16 parallel readout channels to facilitate the rapid testing of micro-organisms/exoelectrogens.

### A. Electrochemical Sensing Module

As shown in Fig. 4, each electrochemical sensing module/potentiostat present in a pixel group consists of three components – a control amplifier, interfacing electrodes and in-pixel transimpedance amplifiers. The control amplifier is responsible for defining the solution potential through the reference electrode and provides the excitation signal to induce an electrochemical response. It regulates the solution potential through the negative feedback loop formed by the interfacing electrodes and the solution medium present between them. The control amplifier is realized using a PMOS-input single stage single-ended op-amp, which provides a DC gain of 29.64 dB. By virtue of containing only one amplification stage, the control amplifier is quite stable under different load conditions in our operation bandwidth (50mHz to 1MHz). Fig. 5 shows the testbench used to test the stability of the potentiostat as well as the circuit model of the electrode-electrolyte interfacial impedance. The values of the parameters listed in Fig. 5(b) were extracted using an off-the-shelf potentiostat (SP-300). Fig. 6 shows the loop gain and loop phase of the loaded potentiostat as well as a histogram of the extracted phase margins. For these plots, the critical parameters of the equivalent circuit model were varied over 2 orders of magnitude around the extracted values. The plots demonstrate that the potentiostat has sufficient phase margin under a wide range of practical loading conditions. The PMOS input transistors and the reduced transistor count of the single stage amplifier result in an inhrently low output noise.

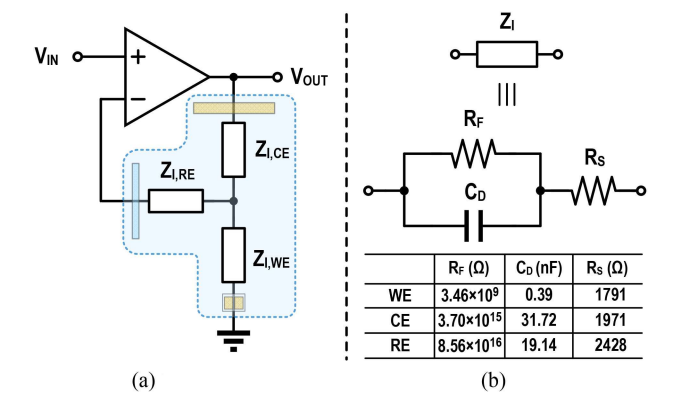


Fig. 5. (a) Simulation testbench for potentiostat (b) Interfacial impedance model along with the extracted values of parameters.

The counter and reference electrodes, connected to the control amplifier, are strategically located near the working electrodes of the sensing pixels to reduce the solution path impedance between all of them. This plays an important role in reducing the voltage drop between the reference and working electrodes through the solution, thus decreasing the difference between the actual and applied excitation signals. For the counter electrodes, their proximity to the working electrodes and their placement on the upper/lower sides of the 4x4 sensing pixel array ensures that most of the current flowing through the sensing pixels also flows through the counter electrodes of that pixel group (Figs. 3 and 4). Moreover, placing the counter electrodes on both upper and lower sides of the 4x4 sensing pixel array ensures that the solution impedances between the counter electrode and the working electrodes in a pixel group are comparable to each other (Fig. 3).

During electrochemical sensing, the sensing pixels are activated sequentially to avoid crosstalk between different pixels and subsequent corruption of the measured data. The two working electrodes of the active sensing pixel are shorted to increase the effective area and hence the measured current. The electrochemical current is sampled by a capacitive transimpedance amplifier (C-TIA), which is also implemented by a PMOS-input single stage op-amp. The low input referred current noise of this topology make it attractive for use in this circuit block.

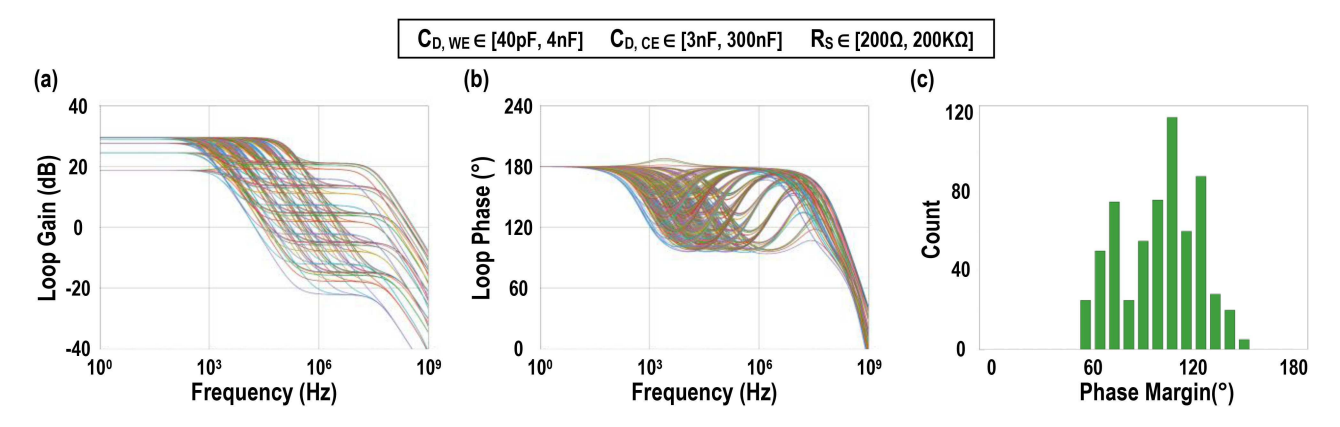


Fig. 6. (a) Loop Gain and (b) Loop Phase plots of the potentiostat loaded with interfacial impedance (c) Histogram of the extracted phase margins.

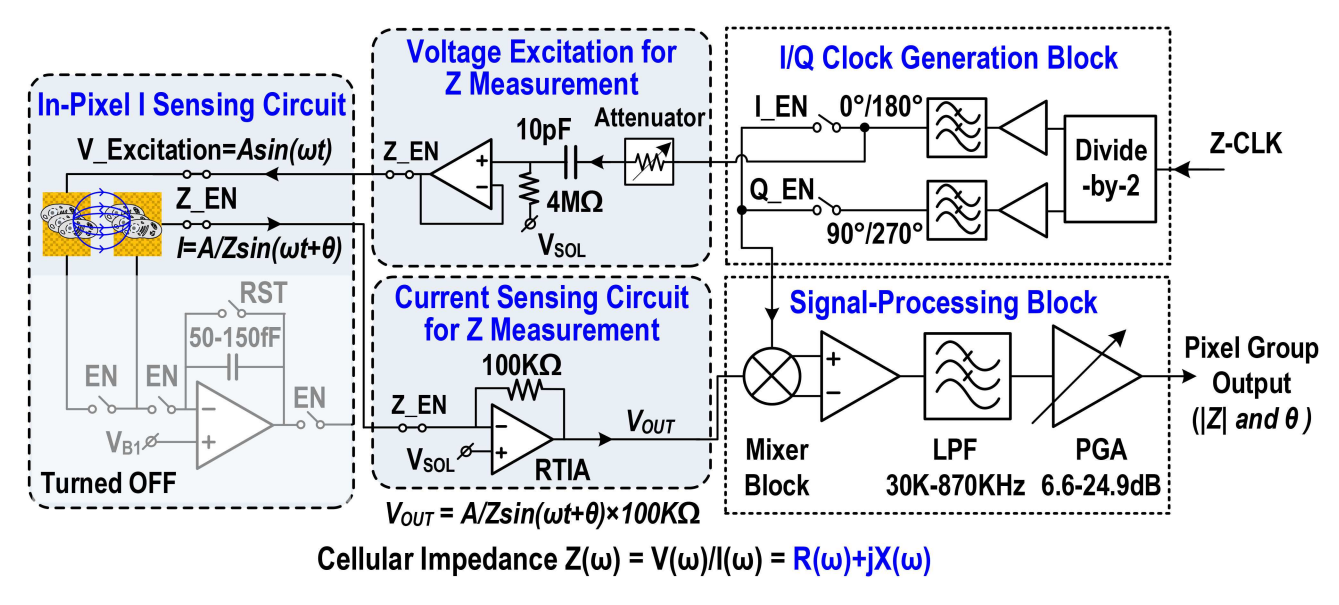


Fig. 7. Circuit diagram of the on-chip impedance sensing module for characterization of cell-to-surface adhesion and biofilm-to-chip adhesion.

The capacitors of the C-TIA are implemented on chip and the total capacitance can be tuned from 50fF to 150fF using 2-bit control signals. The values of these capacitors were chosen based on prior discrete experiments conducted with exoelectrogenic *Shewanella oneidensis* MR-1 bacteria. With a low current noise at its input and a tunable capacitance to adjust its gain, the C-TIA can measure currents ranging from a few pA to several nA, providing a sufficient current sensing dynamic range for exoelectrogen characterizations. To further improve the sensor's noise performance, we employ a 2-point slope extraction technique to calculate the electrochemical current from the measured data (Fig. 4). This technique reduces the effect of flicker noise and DC offset on the extracted electrochemical current by sampling the waveform/signal from the integrator twice in quick succession.

### B. Cellular Impedance Sensing Module

The different circuit blocks involved in complex impedance detection are shown in Fig. 7. When a sensing pixel is configured for complex impedance detection, one of its two working electrodes provides a voltage excitation signal while the other measures the current flowing between the two of them. The source for the voltage excitation is an externally-provided clock signal, denoted by Z-CLK in Fig. 7. Z-CLK is fed to a digital divide-by-2 logic circuit that generates two clock signals that are 90° phase-shifted with respect to each other. These signals are sent to a 6-bit low pass filter; similar to the one present in the signal-processing block; to produce in-phase and quadrature-phase sinusoidal signals. The in-phase sinusoidal signal is used for voltage excitation and is sent to the voltage buffer driving the excitation electrode, while a copy of both the in-phase and quadrature phase signals are fed to the mixer (in the detection chain). Before the in-phase sinusoidal signal is sent to the excitation electrode, it undergoes attenuation to decrease its amplitude to a level at which the electrode avoids any undesirable electrochemical reaction with the solution. A 5-bit attenuator is used for this purpose, capable of providing a maximum attenuation of 42 dB. The output of the attenuator is fed to the voltage buffer, which is responsible for delivering the excitation signal to the electrode and for setting its DC operating point. The current produced due to this voltage excitation flows through the other electrode into a resistive transimpedance amplifier (R-TIA).

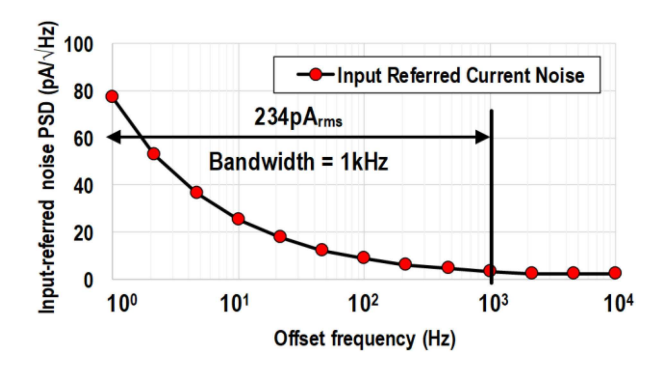


Fig. 8. Simulated Input Referred Current Noise of the Impedance Sensing Module

Like the voltage buffer, the R-TIA also sets the DC bias point for its adjoining working electrode in addition to performing current to voltage conversion. The output of the R-TIA is sent to the fully differential mixer, which performs coherent demodulation of the measured signal and extracts its real and imaginary components. The processed signals are filtered and amplified by the subsequent low-pass filter and programmable-gain amplifier (PGA) stages to produce the required outputs.

For voltage excitation, the excitation amplitude and frequency are chosen such that the impedance change due to the presence of a cell/biofilm can be easily discerned without saturating the current detection chain. Also, as mentioned earlier, we have an additional constraint on the maximum excitation amplitude to prevent any undesired electrochemical reaction between the electrode and the sample solution. Prior experiments performed with some of the other CMOS-based biosensing platforms designed by the group [36]-[39] showed that an amplitude of 50mV proved to be sufficient for detecting the required impedance difference. The flexibility to operate at such low excitation voltages is made possible by the large tunable gain as well as the low input referred current noise of the current detection chain. The impedance sensing module is capable of providing a maximum transimpedance gain of 160 M $\Omega$ , with the individual contributions of the R-TIA, mixer and PGA stages being  $100 \text{ k}\Omega$ , 39.5 dB and 24.6 dB respectively. The simulated input referred current noise of the impedance sensing module is shown in Fig. 8. We see that over a 1 kHz bandwidth, the integrated input current noise is 234 pArms. We choose the operating frequency for cellular impedance measurement to be between 20kHz-500kHz.

# III. IN-HOUSE POST PROCESSING FOR IMPROVED ELECTROCHEMICAL SENSING & CHIP BIOCOMPATIBILITY

The on-chip electrodes of the foundry-fabricated CMOS ICs need to undergo surface modifications to improve their biocompatibility and also their own reliability and integrity, especially during long-term biological experiments (Fig. 9). The additional post-processing steps are indispensable for the contact-based sensing modalities, since the default on-chip electrodes are often made of Aluminum (Al); the top/pad metal layer in standard CMOS processes; which will readily react with common cell culture mediums and buffer solutions. The damage to the Al

electrodes will be rapid and irreversible, rendering them useless in a matter of minutes. Moreover, the faradaic current generated due to these reactions will interfere with the measured currents and disrupt the normal operation of the sensing modalities. Furthermore, the dissolved Al ions are toxic to most cellular cultures.

A common fabrication approach to tackle this issue involves coating the electrodes with an inert layer of gold using the electro-less gold-plating method. In this chemical postprocessing technique, a metal stack of a Zn/Ni/Au is deposited on top of the Allayer native to the CMOS process. This technique has been used by a number of CMOS sensor arrays [37]-[41], and it has shown reasonable success in preventing electrode degradation. However, as this fabrication process deposits gold chemically, the thickness of the gold coating is inversely proportional to the area of each individual electrode. Thus, for large electrodes, like the counter/reference electrodes on our reported chip, the gold coating often cannot cover the entire electrodes uniformly, leading to exposure of underlying Al layer to the solution. To illustrate the risk posed by this issue, we test the long-term reliability of some of our CMOS sensor array chips with electro-less gold-plating on the on-chip electrodes. The chips are immersed in a standard phosphate buffer solution (DPBS) and their condition is observed periodically under a Leica DVM6 digital microscope (Fig. 10). We notice distinct bubbles at the edges of many counter electrodes after a 3.5-hour exposure to DPBS, which only grew larger after another 3 hours. These observations are indicative of an inadequate amount of gold at the edges of the larger electrodes and demonstrate the reliability issue of electro-less gold plating on large on-chip electrodes.

Since the root cause of the biocompatibility issues is the presence of Al in the top metal layer, we have developed a fabrication protocol in which all of the Al in the electrodes is eradicated, hence eliminating the possibility of any unwanted reaction. The fabrication of the on-chip electrodes is carried out in two stages, starting with an initial stage; in which all the electrodes are subjected to the same post-processing steps; followed by a second stage; consisting of steps specific to the fabrication of the reference electrodes. The rest of this paragraph describes the post-processing steps common to all the on-chip electrodes, i.e., the first stage. The CMOS chip is first glued to a thin glass slide using polydimethylsiloxane (PDMS) to facilitate fabrication. Photoresist is then spin-coated onto the chip after which it is patterned using a maskless aligner (Heidlberg MLA150). The pattern exposes the chip's sensing area while leaving the rest of the chip covered. The entire glass slide is then immersed in an Al etchant till all the Al in the electrodes is consumed. Finally, a 200nm thick layer of gold is deposited on all the electrodes using E-beam evaporation, with a thin film of Titanium between the gold layer and the via contact serving as the adhesion layer (Fig. 9).

After the completion of the above set of steps, we begin the fabrication of the on-chip reference electrodes. For the initial electrochemical experiments that we performed with the chip, we used the gold reference electrode that we obtained from the previous processing steps. Some of those results have also

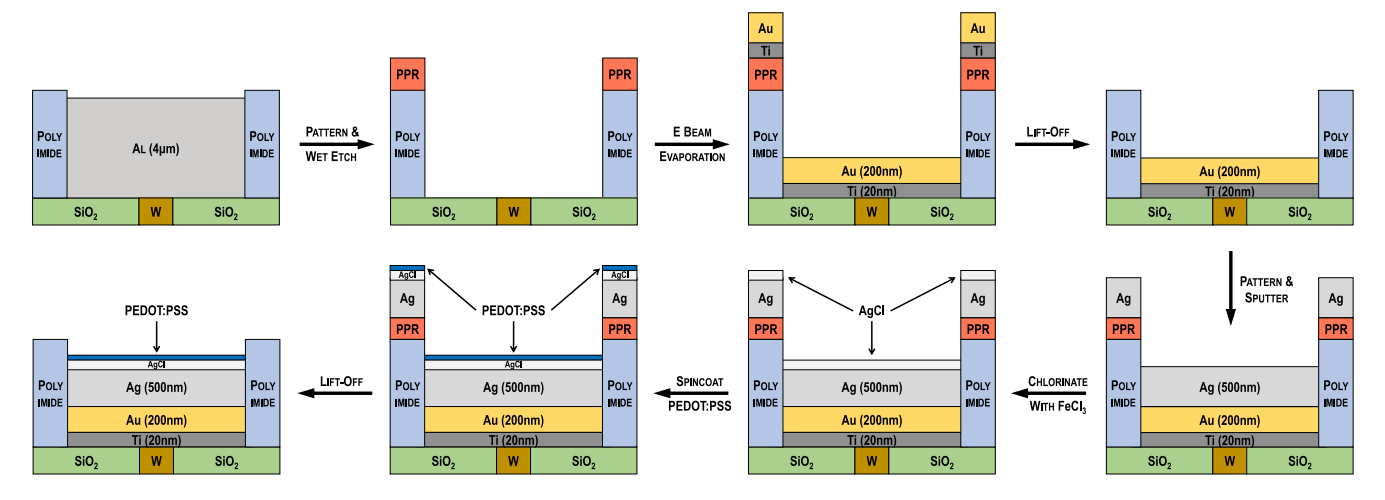


Fig. 9. Fabrication steps for the on-chip PEDOT:PSS coated Ag/AgCl reference electrodes.

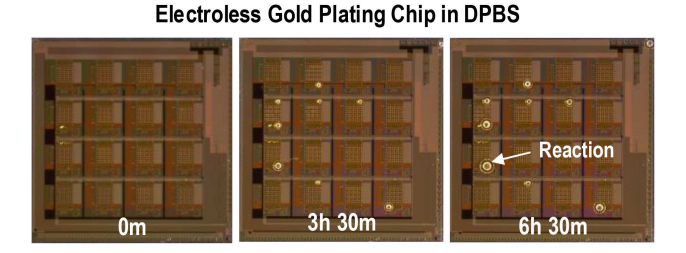


Fig. 10. Electroless gold plated electrodes reacting with DPBS buffer after long periods of time.

been presented in this paper. However, we eventually chose to implement the reference electrodes using an Ag/AgCl stack as it has a stable electrode potential, which improves the reliability and accuracy of the subsequent electrochemical measurements [42], [43]. Due to the cytotoxic nature of silver and the Cl leaching that causes electrode instability, we cannot use the bare solid Ag/AgCl electrodes directly to perform biological experiments. Hence, we coat them with a thin layer of PEDOT:PSS to isolate the biosamples from the Ag/AgCl electrodes, making the reference electrodes biocompatible. The fabrication protocol for the reference electrodes is described in the following sentences (Fig. 9). First, the chip is patterned to expose only the reference electrodes, after which, a thick layer of silver is sputter-deposited on top of them. Next, the top surface of the Ag layer is converted to AgCl by immersing the chip in a 50mM FeCl<sub>3</sub> solution for 30-40 seconds. Once chlorination is complete, we perform a second patterning step to prepare the chip for PEDOT:PSS coating. The solution mixture for the PEDOT:PSS coating is prepared using the chemical composition provided in [44]. The solution is spin-coated on the glass slide at 2000 rpm for 30 seconds and baked at 120°C for 1 hour to yield a layer of PEDOT: PSS that was approximately 220nm thick. Fig. 11 shows the microscopic images of the chip, taken after each key step of the post-processing protocol.

The chips post-processed by the protocol described in the above paragraphs are subjected to the same reliability test that we performed on the electro-less gold-plated chips. We observe no bubbles forming and no unwanted chemical reactions on the chip surface over a 24-hour observation period. Apart from improving the biocompatibility of the electrodes, the Al-free post-processing approach has a shorter lead time and provides a better fabrication yield when compared to the electro-less gold-plating method. In addition to analyzing the surface integrity of the electrodes in salt solution, we also characterize the improvement in electrochemical sensing performance provided by the fabricated Ag/AgCl reference electrodes. We measured the drift in the open circuit voltage (OCV) between a fabricated Ag/AgCl electrode and a standard off-the-shelf Ag/AgCl reference electrode. The fabricated Ag/AgCl electrode for the above OCV experiment was fabricated on a glass wafer using the same post-processing steps that we adopted for the on-chip reference electrode. Fig. 12 shows a microscopic image of the Ag/AgCl electrode as well as the OCV plots. The fabricated Ag/AgCl electrode shows an average drift of only around 1.4 mV/hr over a span of 2 days, which is adequately small considering the timescales of the biological experiments (30 minutes).

After completion of all the fabrication steps, the CMOS chip is carefully detached from the glass slide and wire-bonded to a daughter FR4 PCB. Since the wirebonds and the chip pads will react with culture medium, they are sealed from the external environment using medical epoxy (302-3M, EPOTEK). For the chips used in the chemical/biological experiments, we attached a petridish to the daughter PCB to hold the test samples. Before attachment, the base of the petridish is cut open to accommodate the wirebonded chip, after which it is glued to the PCB using PDMS. A final layer of PDMS covers all the region around the sensing area of the chip to provide additional biocompatibility and protection.

### IV. ELECTRICAL AND BIOLOGICAL MEASUREMENTS

The multi-modal CMOS IC was fabricated in 130nm BiC-MOS process. Fig. 13 shows the chip microphotograph as well as the packaged daughterboard. The measurement setups for the different experiments performed on our CMOS platform are shown in Fig. 14. In all of the measurements, the daughter PCB

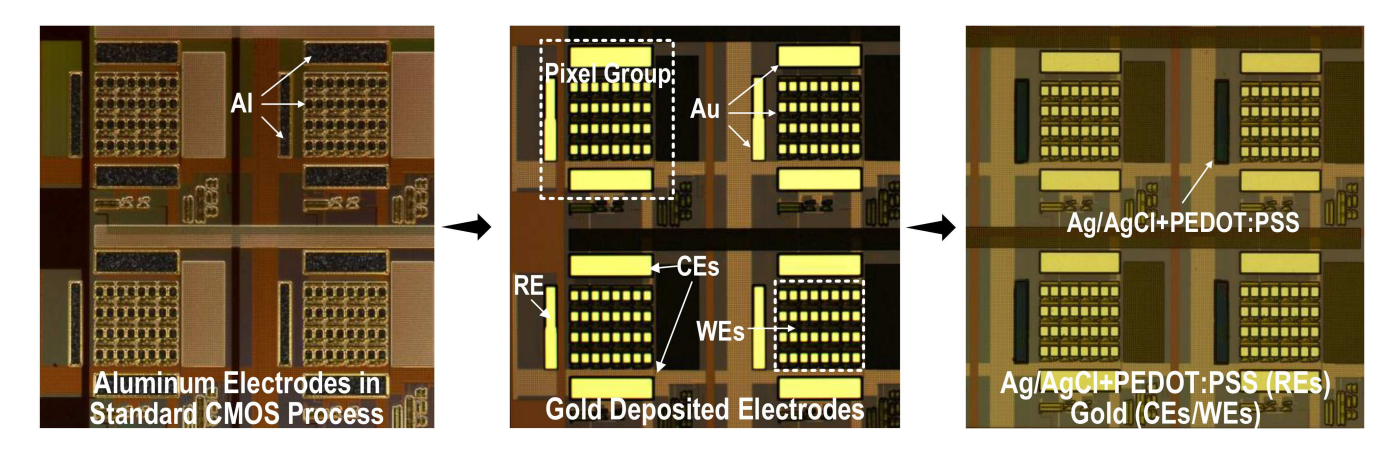


Fig. 11. Microscopic Images of the multi-modal CMOS chip taken after key fabrication stages.

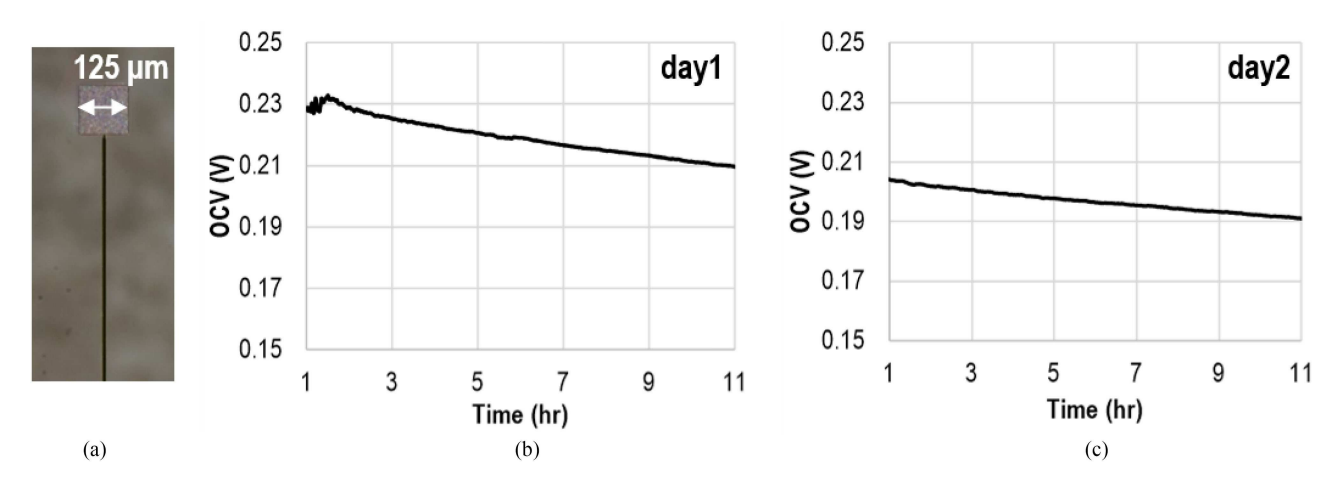


Fig. 12. (a) Microscopic image of the Ag/AgCl/PEDOT:PSS reference electrode used for the OCV tests (b), (c) OCV plots of the fabricated reference electrodes measured over 10 hour windows for 2 days (right).

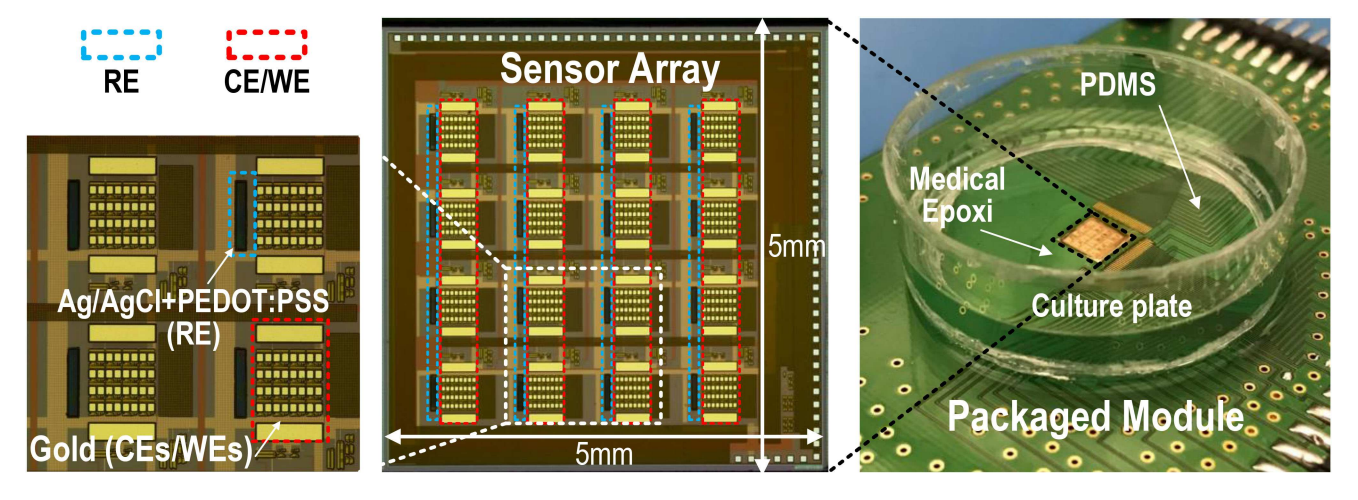


Fig. 13. Chip microphotographs of the post-processed chip and the fully packaged module.

holding the fully packaged CMOS sensor array is connected to the mother PCB, which provides the supply voltages and the various reference voltages required for proper functioning of the chip. The CMOS IC is programmed using an FPGA (USB-1616HS, Measurement Computing Corp.) which writes

the configuration bits into the CMOS chip's serial-to-parallel digital programming interface (SPI). The same FPGA is used to read the analog outputs of the IC and digitize them for subsequent data processing by a personal computer. For the electrochemical experiments with the exoelectrogens, we replace

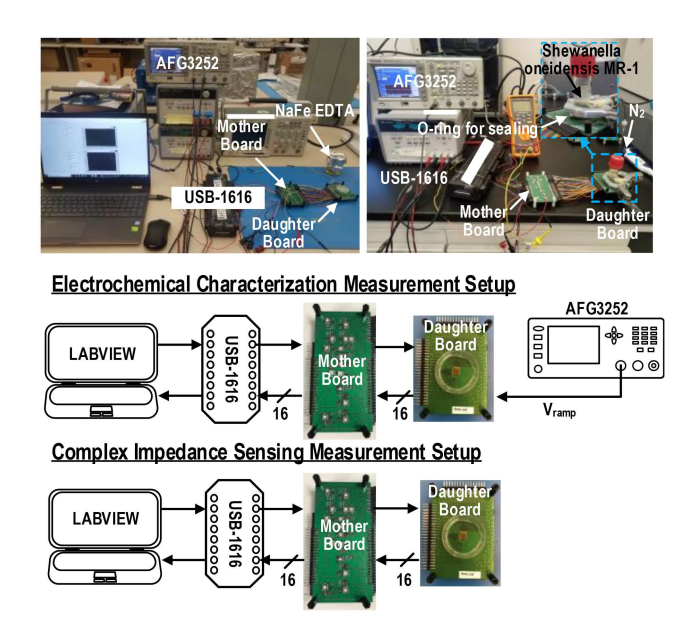


Fig. 14. Measurement setup for the various chemical and biological experiments.

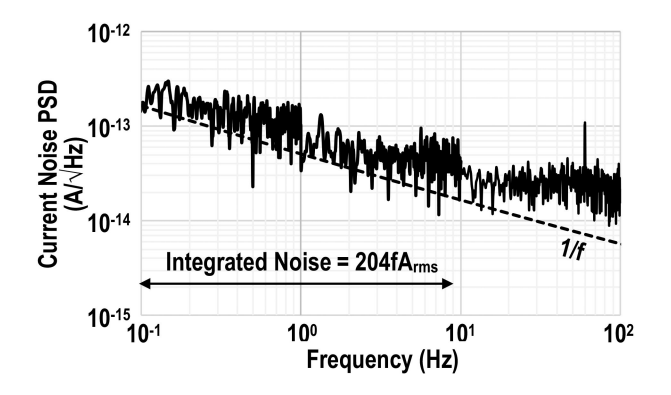


Fig. 15. Input Referred Current Noise Amplitude Spectral Density (ASD) of the electrochemical current readout circuits.

the petridish on the daughter PCB with a bottomless reactor (inset Fig. 14, top right) to hold the sample solution. The gap between the reactor and the PCB is sealed using a combination of clamps and a rubber o-ring to prevent the solution from leaking. Nitrogen gas is constantly bubbled into the sample solution to displace any oxygen that is present as it can interfere with the electrochemical signal coming from the exoelectrogens.

In order to ascertain the optimal values of the various experimental parameters for the biological tests (e.g., excitation frequency, excitation amplitude, bacterial concentration), we first performed a series of electrical tests to identify the detection limits of the different sensing blocks present on chip. For the electrochemical sensing modality, we characterized the noise performance of its current detection chain to determine the electrochemical current sensitivity of the proposed CMOS IC. The input-referred current noise of the current detection chain was measured using a dynamic signal analyzer (Keysight 35670A) and its amplitude spectral density is shown in Fig. 15. The rms current noise in our bandwidth of interest (0.1Hz to 10 Hz) is

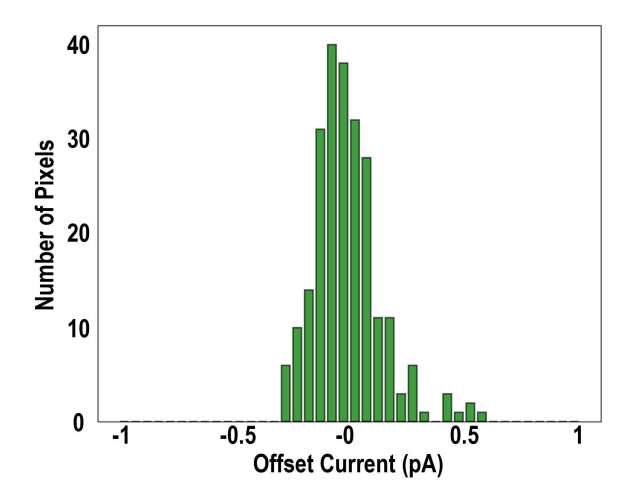


Fig. 16. Histogram of leakage current through C-TIA switch.

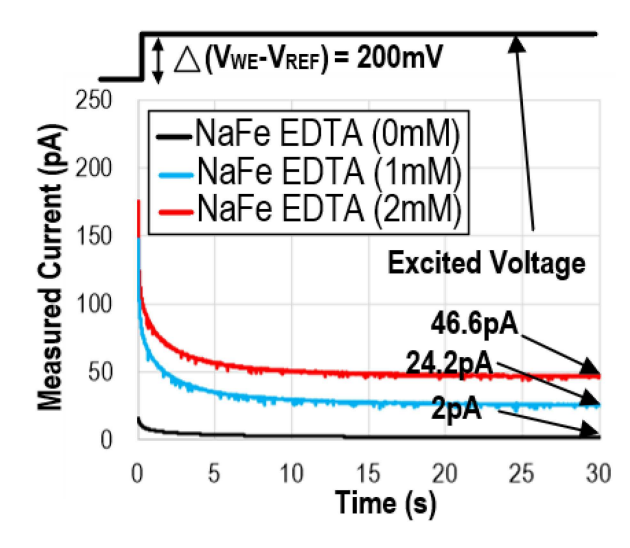


Fig. 17. Chronoamperometry (CA) experiments with different concentrations NaFeEDTA.

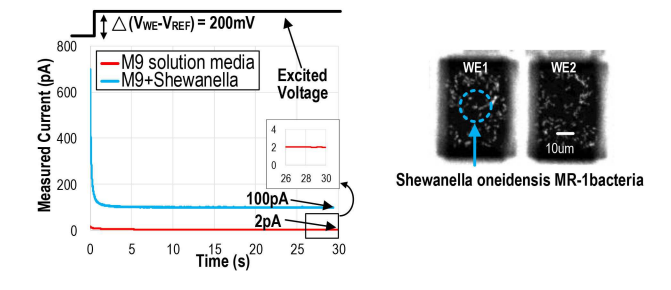


Fig. 18. CA response of Shewanella Oneidensis MR-1 bacteria (left) and the microscopic image of the fluorescent-labelled bacteria (right).

204fA rms, which allows accurate sensing of down-to pA-level electrochemical current coming from a cluster of bacteria cells. As one can infer from the plot in Fig. 15, the rms current noise in electrochemical sensing circuits is typically dominated by the low frequency flicker noise.

Another source of signal distortion for the electrochemical measurements is the leakage current through the integrator switch. We measured the leakage current flowing through multiple sensing pixels and obtained an average leakage current of

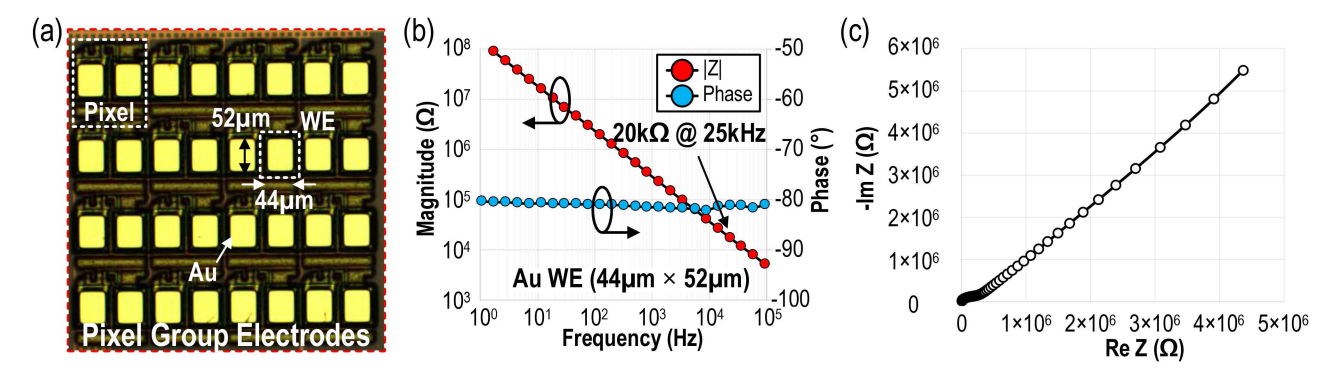


Fig. 19. (a) Close up of the gold plated sensing pixels (b) EIS plots of the electrodes in DPBS (c) Nyquist plot of the electrodes.

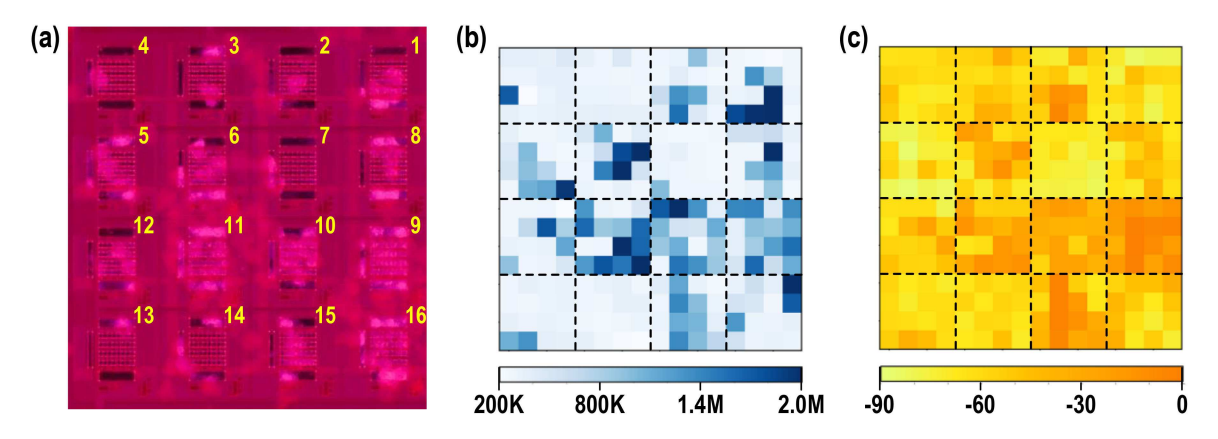


Fig. 20. (a) Microscopic image of full chip covered with HEK-293 cell clusters (b) Impedance magnitude map of entire chip (c) Impedance phase map of entire chip.

275 fA. Fig. 16 shows the distribution of the leakage currents about their mean value, with most pixels exhibiting/displaying a leakage current that was within 0.5pA of the average.

For the electrochemical experiments, we first tested the chip against a well-characterized electroactive compound to verify the proper operation of the chip's electrochemical sensing module. For this purpose, the chemical NaFeEDTA was chosen due to its harmless nature. We first performed chronoamperometry, an electrochemical test in which a voltage pulse is applied between the working and reference electrodes and the electrochemical current generated at the working electrode is measured. CA experiments were performed with different concentrations of the analyte using a polarization voltage of 0.2V, and the measured currents are plotted in Fig. 17. The results obey Cottrell's equation, which states that the current in the diffusioncontrolled regime (i.e., for  $\Delta V >> V_{OX}$ ) is proportional to the concentration of the analyte at any given time. The electrochemical currents at the end of the 30 second experimental duration are labelled, showing a clear linear increase in current with concentration. For the above experiments, chips containing gold reference electrodes were used. Since we were observing the variation of electrochemical current with concentration, the choice of reference electrode for these experiments was not critical.

After completion of the preliminary set of electrochemical tests with NaFeEDTA, we began the biological experiments

with Shewanella oneidensis MR-1, a class of exoelectrogenic bacteria. We characterized the current generating capacity of a genetic variant of these microbes through CA experiments. For these experiments, we made use of the CMOS chips with gold reference electrodes. The sample solutions for the tests were composed of M9 salt solution (microbial growth medium), lactate (food) and the exoelectrogenic bacteria. We applied a 0.2V excitation signal to a sample containing  $15x10^8$  cells/ $\mu$ L of the Shewanella oneidensis bacteria and measured the electrochemical current generated. This current is compared to the current produced from a sample that does not contain the bacteria. From Fig. 18, we see a clear difference between the two currents, with the current measured from the bacterial sample being more than an order higher in magnitude. Hence, we can clearly detect the presence of the current-generating bacteria using the chip. The current density generated by the bacteria at the end of the CA experiment is 22 mA/m<sup>2</sup>, which is within the range of the current densities on Au electrodes reported in literature [45].

For impedance sensing experiments, before we began the biological tests, we performed electrochemical impedance spectroscopy (EIS) measurements of gold-plated electrodes in DPBS solution to determine a suitable stimulation frequency for impedance detection. Fig. 19 shows the Bode and Nyquist plots of the electrodes immersed in solution. We choose a frequency of 25 KHz to stimulate the cell samples as the impedance at this frequency is considerably lower than the typical cell-electrode

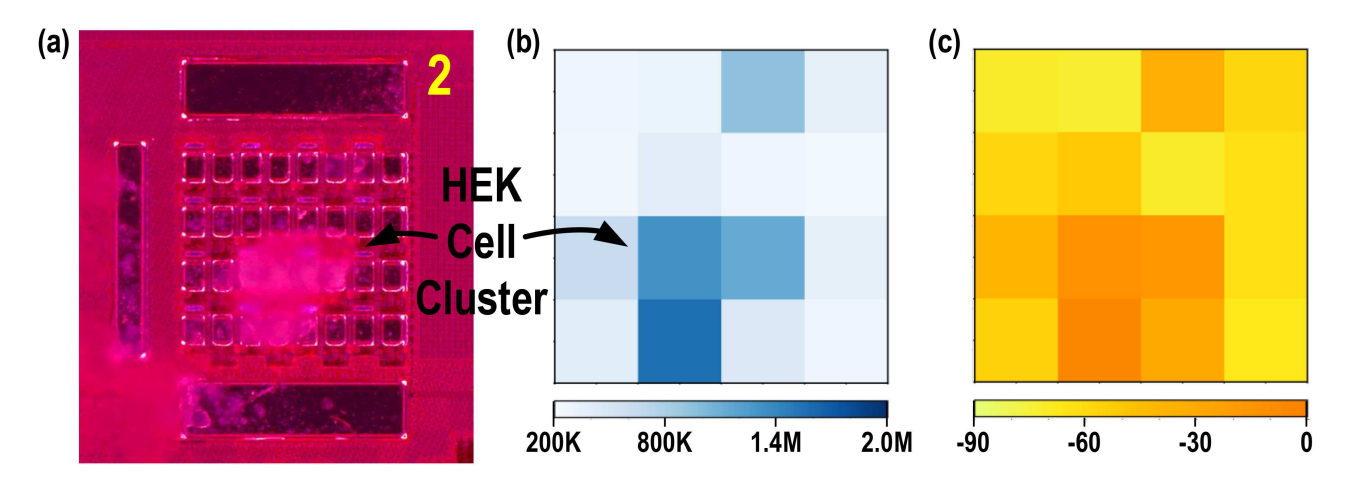


Fig. 21. (a) Microscopic image of pixel-group 2 (b) Impedance magnitude map of pixel-group 2 (c) Impedance phase map of pixel-group 2.

 ${\it TABLE~I}$  Comparison Table of State of the Art CMOS Electrochemical and Impedance Biosensors

	This Work	TBCAS 2010 A. Manickam [5]	JSSC, 2014 H. M. Jafari [6]			JSSC, 2008 P. M. Levine [7]	ISSCC, 2019 A. Manickam [8]
Modality	Electrochemical Current Sensing + Complex Z Sensing	Z sensing*	Electrochemical Current Sensing			Electrochemical Current Sensing	Electrochemical Current Sensing
# of Electrodes (RE, CE, WE)	16, 32, 512	1**, N/A, 100 (Potentiostat absent)	1**, 1, 54			1 <sup>**</sup> , 1, 16	1, 1, 1024
Pixel Size (µm²)	100×100	90×90	2×2	5×5	55×55	70×70, 80×80, 90×90,100×100	100×100†
Sensitivity (pA)	0.204	330	8.6	132	1050	240	0.28
I <sub>max</sub> (nA)	59.9	N/A	350			250	12.5
Field-of-View (mm²)	3.2×3.72	0.9×0.9	N/A			N/A	3.2×3.2
# of Channels	16	1	1			16	2
Electrode Material	Ag/AgCI+PEDOT:PSS (RE) Ti/Au (CE/WE)	Au (RE) Al/Ni/Au (WE)	Ag/AgCl (RE) Al/Ni/Pd/Au (CE/WE)			Ag/AgCI (RE) Ti/Au (CE/WE)	AI/Ti/a-C (RE/CE/WE)
Reference Electrode	On-Chip	Off-Chip	Off-Chip			Off-Chip	On-Chip
Readout Speed (kHz)	1000	0.109	3.4			2.5	0.05
Assay Type	Exoelectrogen Bacteria, HEK-293 Cancer Cells	DNA, Protein	DNA			DNA	DNA
Power (mW)	2.25/pixel group	84.8	0.042/pixel			10 <sup>††</sup>	0.25/pixel
Process (nm)	130	350	130			250	250

†include RE, CE, and WE. †† Approximated value. \* External excitation electrode. \*\* Off-chip reference electrode.

impedance, which can range from several 100 K $\Omega$  to a few M $\Omega$ . For the biological testing of the impedance modules, we cultured HEK-293 cancer cell clusters on our chips. After the cells were seeded on the chip surface, they were left to proliferate for a couple of days before the impedance scan of the chip was performed. Fig. 20 shows the microscopic image of a HEK-293 seeded chip juxtaposed with the corresponding 2-D impedance magnitude and phase maps obtained from the impedance sensors on chip. Fig. 21 shows the corresponding microscopic images and impedance maps for a single pixel group (pixel-group 2). From these images, we observe a good correlation between the cell locations in the microscopic image and the high impedance zones in the impedance map, verifying the proper operation of the impedance sensing blocks on chip. These results show that

the impedance sensing modality can be used to obtain information on the distribution of the various cells on the chip. Hence, one can use this knowledge in tandem with the electrochemical experiments to identify the stimulation sites for electrochemical sensing that can provide the highest SNR.

### V. CONCLUSION

This paper presented a CMOS multi-modality sensor array housing electrochemical and impedance sensing blocks along with 256 sensing pixels for high-throughput characterization of exoelectrogens. The reported CMOS chip underwent additional fabrication steps to boost the biocompatibility of the on-chip e lectrodes. The adopted fabrication protocol produced electrodes

which were considerably more stable in solution media when compared to the electrodes obtained from electroless gold plating, and this improvement in stability is mainly attributed to the elimination of Aluminum in the top metal layer. The noise measurements of the chip's electrochemical sensors highlight the low input-referred current noise of the sensor, showing that the chip is capable of measuring the minute pA-level electrochemical currents that are generated by a small group of exoelectrogenic cells. The chemical experiments performed with the redox active analyte NaFeEDTA verified the proper functioning of the electrochemical sensing blocks. The subsequent biological experiments with the exoelectrogen Shewanella oneidensis MR-1 yielded meaningful electrochemical results, with the signal coming from the bacteria sample being a couple orders higher than that of the control experiment. The chip was also able to successfully measure the change in interfacial impedance due to the adhesion of HEK-293 cancer cells to the electrodes on chip. The entire chip was scanned to obtain a 2D impedance map of the cultured cells, and the regions of high impedance corresponded to the cell locations in the fluorescent microscopic image. Hence, the proposed CMOS platform can extract high resolution, multi-dimensional sensory information, potentially at a high throughput, making it a superior alternative to traditional setups that employ large reactors and bulky off-the-shelf equipment. Table I lists the various state-of-the-art CMOS electrochemical and impedance sensing platforms. The proposed CMOS IC exhibits excellent current sensitivity and the unique combination of the on-chip sensors enables multidimensional characterization of exoelectrogens. In the future, we hope to integrate the IC with a microfluidics structure, which will reduce the sample volume to a few  $\mu l$  and isolate multiple samples on the same chip, allowing us to fully exploit the chip's capabilities.

### ACKNOWLEDGMENT

The authors thank Globalfoundries for CMOS sensor array chip fabrication and members at Georgia Tech Electronics and Micro-System (GEMS) lab for their helpful discussions. Any opinions, findings, and conclusions or recommendations expressed in this material are those of the author(s) and do not necessarily reflect the views of the U.S. Office of Naval Research or the National Science Foundation.

#### REFERENCES

- M. A. TerAvest and C. M. Ajo-Franklin, "Transforming exoelectrogens for biotechnology using synthetic biology," *Biotechnol. Bioeng.*, vol. 113, no. 4, pp. 687–697, 2016.
- [2] B. E. Logan, "Exoelectrogenic bacteria that power microbial fuel cells," *Nature Rev. Microbiol.*, vol. 7, no. 5, pp. 375–381, 2009.
- [3] B. E. Logan, R. Rossi, and P. E. Saikaly, "Electroactive microorganisms in bioelectrochemical systems," *Nature Rev. Microbiol.*, vol. 17, no. 5, pp. 307–319, 2019.
- [4] S. V. Mohan, R. Saravanan, S. V. Raghavulu, G. Mohanakrishna, and P. Sarma, "Bioelectricity production from wastewater treatment in dual chambered microbial fuel cell (MFC) using selectively enriched mixed microflora: Effect of catholyte," *Bioresour. Technol.*, vol. 99, no. 3, pp. 596–603, 2008.

- [5] B. Zhang, H. Zhao, S. Zhou, C. Shi, C. Wang, and J. Ni, "A novel UASB–MFC–BAF integrated system for high strength molasses wastewater treatment and bioelectricity generation," *Bioresour. Technol.*, vol. 100, no. 23, pp. 5687–5693, 2009.
- [6] L. Zhuang, Y. Zheng, S. Zhou, Y. Yuan, H. Yuan, and Y. Chen, "Scalable microbial fuel cell (MFC) stack for continuous real wastewater treatment," *Bioresour. Technol.*, vol. 106, pp. 82–88, 2012.
- [7] B. E. Logan and K. Rabaey, "Conversion of wastes into bioelectricity and chemicals by using microbial electrochemical technologies," *Science*, vol. 337, no. 6095, pp. 686–690, 2012.
- [8] P.-L. Tremblay and T. Zhang, "Electrifying microbes for the production of chemicals," Front. Microbiol., vol. 6, p. 201, 2015.
- [9] Y. J. Shen, O. Lefebvre, Z. Tan, and H. Y. Ng, "Microbial fuel-cell-based toxicity sensor for fast monitoring of acidic toxicity," *Water Sci. Technol.*, vol. 65, no. 7, pp. 1223–1228, 2012.
- [10] D. Yu, L. Bai, J. Zhai, Y. Wang, and S. Dong, "Toxicity detection in water containing heavy metal ions with a self-powered microbial fuel cell-based biosensor," *Talanta*, vol. 168, pp. 210–216, 2017.
- [11] M. A. TerAvest, Z. Li, and L. T. Angenent, "Bacteria-based biocomputing with cellular computing circuits to sense, decide, signal, and act," *Energy Environ. Sci.*, vol. 4, no. 12, pp. 4907–4916, 2011.
- [12] B. D. DeBusschere and G. T. Kovacs, "Portable cell-based biosensor system using integrated CMOS cell-cartridges," *Biosensors Bioelectron.*, vol. 16, no. 7/8, pp. 543–556, 2001.
- [13] M. Mimee et al., "An ingestible bacterial-electronic system to monitor gastrointestinal health," *Science*, vol. 360, no. 6391, pp. 915–918, 2018.
- [14] G. Choi, D. J. Hassett, and S. Choi, "A paper-based microbial fuel cell array for rapid and high-throughput screening of electricity-producing bacteria," *Analyst*, vol. 140, no. 12, pp. 4277–4283, 2015.
- [15] G. Choi and S. Choi, "Monitoring electron and proton diffusion flux through three-dimensional, paper-based, variable biofilm, and liquid media layers," *Analyst*, vol. 140, no. 17, pp. 5901–5907, 2015.
- [16] R. Mahadevan et al., "Characterization of metabolism in the Fe (III)reducing organism geobacter sulfurreducens by constraint-based modeling," Appl. Environ. Microbiol., vol. 72, no. 2, pp. 1558–1568, 2006.
- [17] M. H. Serres and M. Riley, "Genomic analysis of carbon source metabolism of Shewanella Oneidensis MR-1: Predictions versus experiments," *J. Bacteriol.*, vol. 188, no. 13, pp. 4601–4609, 2006.
- [18] S. Xu and H. Liu, "New exoelectrogen Citrobacter sp. SX-1 isolated from a microbial fuel cell," *J. Appl. Microbiol.*, vol. 111, no. 5, pp. 1108–1115, 2011
- [19] M. Lienemann et al., "Towards patterned bioelectronics: Facilitated immobilization of exoelectrogenic Escherichia Coli with heterologous pili," Microbial Biotechnol., vol. 11, no. 6, pp. 1184–1194, 2018.
- [20] J. Carrera and M. W. Covert, "Why build whole-cell models?," *Trends Cell Biol.*, vol. 25, no. 12, pp. 719–722, 2015.
- [21] C. J. Petzold, L. J. G. Chan, M. Nhan, and P. D. Adams, "Analytics for metabolic engineering," Front. Bioeng. Biotechnol., vol. 3, pp. 135, 2015
- [22] C. P. Goldbeck *et al.*, "Tuning promoter strengths for improved synthesis and function of electron conduits in Escherichia Coli," *ACS Synthetic Biol.*, vol. 2, no. 3, pp. 150–159, 2013.
- [23] S.-J. Yuan et al., "A plate-based electrochromic approach for the high-throughput detection of electrochemically active bacteria," Nature Protocol, vol. 9, no. 1, p. 112, 2014.
- [24] S.-J. Yuan et al., "A photometric high-throughput method for identification of electrochemically active bacteria using a WO 3 nanocluster probe," Sci. Rep., vol. 3, p. 1315, 2013.
- [25] S. N. Krylov et al., "Instrumentation for chemical cytometry," Anal. Chem., vol. 72, no. 4, pp. 872–877, 2000.
- [26] L. A. Herzenberg, D. Parks, B. Sahaf, O. Perez, M. Roederer, and L. A. Herzenberg, "The history and future of the fluorescence activated cell sorter and flow cytometry: A view from Stanford," *Clin. Chem.*, vol. 48, no. 10, pp. 1819–1827, 2002.
- [27] S. Gawad, L. Schild, and P. Renaud, "Micromachined impedance spectroscopy flow cytometer for cell analysis and particle sizing," *Lab Chip*, vol. 1, no. 1, pp. 76–82, 2001.
- [28] F. J. Blanco et al., "Microfluidic-optical integrated CMOS compatible devices for label-free biochemical sensing," J. Micromechanics Micro-Eng., vol. 16, no. 5, p. 1006, 2006.
- [29] A. Manickam, A. Chevalier, M. McDermott, A. D. Ellington, and A. Hassibi, "A CMOS electrochemical impedance spectroscopy biosensor array for label-free biomolecular detection," in *Proc. IEEE Int. Solid-State Circuits Conf.*, 2010, pp. 130–131.

- [30] H. Wang, Y. Chen, A. Hassibi, A. Scherer, and A. Hajimiri, "A frequency-shift CMOS magnetic biosensor array with single-bead sensitivity and no external magnet," in *Proc. IEEE Int. Solid-State Circuits Conf. Dig. Tech. Papers*, 2009, pp. 438–439.
- [31] N. Sun, Y. Liu, H. Lee, R. Weissleder, and D. Ham, "CMOS RF biosensor utilizing nuclear magnetic resonance," *IEEE J. Solid-State Circuits*, vol. 44, no. 5, pp. 1629–1643, 2009.
- [32] A. Hassibi and T. H. Lee, "A programmable 0.18-\$\mu\hbox {m} \$ CMOS electrochemical sensor microarray for biomolecular detection," *IEEE Sensors J.*, vol. 6, no. 6, pp. 1380–1388, Dec. 2006.
- [33] R. Kumar, L. Singh, Z. A. Wahid, and M. F. M. Din, "Exoelectrogens in microbial fuel cells toward bioelectricity generation: A review," *Int. J. Energy Res.*, vol. 39, no. 8, pp. 1048–1067, 2015.
- [34] D. Jung et al., "A CMOS multimodality in-pixel electrochemical and impedance cellular sensing array for massively paralleled synthetic exoelectrogen characterization," in Proc. IEEE Int. Solid-State Circuits Conf., 2020, pp. 436–437.
- [35] C. W. Shields IV, C. D. Reyes, and G. P. López, "Microfluidic cell sorting: A review of the advances in the separation of cells from debulking to rare cell isolation," *Lab Chip*, vol. 15, no. 5, pp. 1230–1249, 2015.
- [36] D. Jung et al., "A 21952-pixel multi-modal CMOS cellular sensor array with 1568-pixel parallel recording and 4-point impedance sensing," in Proc. IEEE Symp. VLSI Circuits, 2019, pp. C62–C63.
- [37] J. S. Park et al., "1024-pixel CMOS multimodality joint cellular sensor/stimulator array for real-time holistic cellular characterization and cell-based drug screening," *IEEE Trans. Biomed. Circuits Syst.*, vol. 12, no. 1, pp. 80–94, Feb. 2018.
- [38] J. S. Park et al., "Multi-parametric cell profiling with a CMOS quadmodality cellular interfacing array for label-free fully automated drug screening," Lab Chip, vol. 18, no. 19, pp. 3037–3050, 2018.
- [39] J. S. Park et al., "Intracellular cardiomyocytes potential recording by planar electrode array and fibroblasts co-culturing on multi-modal CMOS chip," *Biosensors Bioelectron.*, vol. 144, p. 111626, 2019.
- [40] C.-L. Hsu, A. Sun, Y. Zhao, E. Aronoff-Spencer, and D. A. Hall, "A 16 × 20 electrochemical CMOS biosensor array with in-pixel averaging using polar modulation," in *Proc. IEEE Custom Integr. Circuits Conf. (CICC)*, 2018, pp. 1–4.
- [41] A. C. Sun, E. Alvarez-Fontecilla, A. Venkatesh, E. Aronoff-Spencer, and D. A. Hall, "High-density redox amplified coulostatic discharge-based biosensor array," *IEEE J. Solid-State Circuits*, vol. 53, no. 7, pp. 2054–2064, Jul. 2018.
- [42] G. J. Janz and H. Taniguchi, "The silver-silver halide electrodes. Preparation, stability, and standard potentials in aqueous and non-aqueous media," *Chem. Rev.*, vol. 53, no. 3, pp. 397–437, 1953.
- [43] B. J. Polk, A. Stelzenmuller, G. Mijares, W. MacCrehan, and M. Gaitan, "Ag/AgCl microelectrodes with improved stability for microfluidics," *Sensors Actuators B Chem.*, vol. 114, no. 1, pp. 239–247, 2006.
- [44] P. Gkoupidenis, N. Schaefer, B. Garlan, and G. G. Malliaras, "Neuromorphic functions in PEDOT: PSS organic electrochemical transistors," *Adv. Mater.*, vol. 27, no. 44, pp. 7176–7180, 2015.
- [45] A. L. Kane, D. R. Bond, and J. A. Gralnick, "Electrochemical analysis of Shewanella Oneidensis engineered to bind gold electrodes," ACS Synthetic Biol., vol. 2, no. 2, pp. 93–101, 2013.



Doohwan Jung (Student Member, IEEE) received the B.S. degree in electrical and electronic engineering from Yonsei University, Seoul, South Korea, in 2011, the M.S. degree from the University of Michigan, Ann Arbor, MI, USA, in 2013, and the Ph.D. degree from the Georgia Institute of Technology, Atlanta, GA, USA. From 2013 to 2015, he was with Samsung Electronics, South Korea, where he designed PLL. He is currently a Postdoctoral Researcher in electrical engineering with the Georgia Institute of Technology, Atlanta, GA, USA. His current research

interests include novel RF and mm-wave integrated circuits, and sensors for biomedical applications. He was the recipient of the Analog Devices Inc., Outstanding Student Designer Award in 2018 and CICC Best Student Paper Award in 2019 (2nd Place). His paper was selected for a Technical Tip Sheet at 2019 VLSI Symposium.



Jong-Seok Park (Member, IEEE) received the B.S. degree (Hons.) in electrical and electronic engineering from Yonsei University, Seoul, South Korea, in 2012, and the Ph.D. degree in electrical and computer engineering from the Georgia Institute of Technology, Atlanta, GA, USA, in 2017. He is currently with Intel Labs, Hillsboro, OR, USA. His current research interests include RF/millimeter-wave integrated circuits and systems for wireless communications, integrated sensors or actuators for biomedical applications, and cryo-CMOS integrated systems for

a large-scale quantum qubit control. He was the recipient of the Study-Abroad Scholarship from the Korea Foundation for Advanced Studies in 2012 and Analog Device Inc., Outstanding Student Designer Award in 2014, Catalyst Foundation, IBM, Intel CICC Student Scholarship Award in 2015, and CICC Best Student Paper Award in 2015. He was the co-recipient of RFIC Best Student Paper Award (first place) in 2014.



Sara Tejedor-Sanz received the B.S. and master's degrees in chemical engineering from the Complutense University of Madrid, Madrid, Spain, in 2009, and the master's degree in hydrology and water resources management in 2011, and the Ph.D. degree in chemical engineering from the University of Alcalá, Madrid, Spain, in 2016. From 2013 to 2014, she was with the Department of Innovation and Technology of the company FCC Aqualia on the development of pilot scale bioreactors. From 2017 to 2018, she trained as a Postdoctoral Fellow with

IMDEA Water Institute with Prof. Abraham Esteve-Núñez. In 2018, she joined as a Postdoctoral Fellow Prof. Caroline Ajo-Franklin Laboratory, Lawrence Berkeley National Laboratory and Rice University, Houston, TX, USA. Her research interests include novel electrode and bioreactor designs to optimize bacteria-electrode interactions, the metabolic and bioenergetic fundaments of electroactive microorganisms, and the applications of microbial electrochemistry in environmental biotechnology, food science, and biomedicine.



Sagar R. Kumashi (Student Member, IEEE) received the B.Tech. and M.Tech. degrees in electronics and electrical communication engineering with specialization in VLSI from IIT Kharagpur (IIT KGP), Kharagpur, India, in 2018. He is currently working toward the M.S. degree in electrical and computer engineering with the Georgia Institute of Technology, Atlanta, GA, USA. His research interests include bioelectronics and integrated sensor systems.



Sandra Grijalva received the B.S. degree in biomedical engineering from the University of Arizona, Tucson, AZ, USA, in 2014, and the Ph.D. degree in biomedical engineering from the joint program between Georgia Institute of Technology and Emory University, Atlanta, GA, USA, in 2017. Her research interests include developing and testing models of engineered biological pacemaker tissues to treat heart rhythm disorders. Her research projects included acquisition and analyses of optical-electrical conduction in heart muscle tissues and detection of spon-

taneous pacemaker activity using micro-electrode arrays. She was awarded the National Institutes of Health F31 Predoctoral Fellowship to conduct this research and was Principal Investigator.



Adam Wang (Student Member, IEEE) received the B.S. degree in electrical engineering and mathematics (Summa Cum Laude) from Vanderbilt University, Nashville, TN, USA, in 2017. He is currently working toward the Ph.D. degree in electrical engineering with the Georgia Institute of Technology, Atlanta, GA, USA. His research interests include bioelectronics, biomaterials, microfabrication, and integrated sensors for biomedical application. He was the recipient of Analog Devices Outstanding Student Designer Award in 2020, National Defense Science and En-

gineering Graduate Fellowship in 2019, and the Presidential Fellowship from Georgia Institute of Technology in 2017.



Sensen Li (Member, IEEE) received the B.Eng. (Hons.) and B.A. degrees from Zhejiang University, Hangzhou, China, in 2013, and the Ph.D. degree from the Georgia Institute of Technology, Atlanta, GA, USA, in 2020. He is currently a Research Engineer with Samsung Research America, Plano, TX, USA, developing the next-generation millimeterwave communication systems. His research interests include RF, mm-wave, and THz integrated antenna, circuit, and system designs for wireless communication, radar, and hyperspectral imaging applications.

He was the recipient of the First-Class Scholarship for Outstanding Undergraduate students (Top 5%), Zhejiang University, Hangzhou, China, the Analog Devices, Inc., Outstanding Student Designer Award in 2018, IEEE Antennas and Propagation Society (AP-S) Doctoral Research Grant in 2018, and IEEE Microwave Theory and Techniques Society (MTT-S) Graduate Fellowship in 2019. His article was selected as Best Student Paper Award (2nd place) at the 2018 IEEE Radio Frequency Integrated Circuits Symposium (RFIC). He was also the co-recipient of IEEE Custom Integrated Circuits Conference (CICC) Best Paper Award in 2019.



Hee Cheol Cho received the Ph.D. degree in cardiac electrophysiology from the University of Toronto, Toronto, ON, Canada, in 2003. During the fellowship with Johns Hopkins from 2003 to 2006, he has pioneered the concept of biological pacemakers as alternatives to electronic cardiac pacemaker devices. This led to an investment of \$1M/year for three years from Medtronic, Inc., to form a venture biotech company in Baltimore, MD, USA, where he was the Director of the R&D program. In 2009, he resumed his academic career with Cedars-Sinai Medical Center,

Los Angeles, CA, USA, and with the University of California, Los Angeles, Los Angeles, CA, USA, as an Assistant Professor. There, he made breakthrough discovery that a single-gene transfer sufficed to create biological pacing in a small and large animal models. In 2014, he joined Emory University, Atlanta, GA, USA, and substantially expanded his research group to advance the concept of biological pacemakers toward clinical reality. He and his team are with Emory Hospital's cardiologists to validate long-term biological pacing in a clinically relevant porcine model of complete heart block. He was the recipient of the Postdoctoral Fellowship training from the the Division of Cardiology, Johns Hopkins Medical Institution.



Caroline Ajo-Franklin received the B.S. degree in chemistry from Emory University, Atlanta, GA, USA, in 1997, and the Ph.D. degree in chemistry from Stanford University, Palo Alto, CA, USA, in 2004. From 2005 to 2007, she trained as Postdoctoral Fellow with Prof. Pam Silver with the Department of Systems Biology, Harvard Medical School, Cambridge, MA, USA. From 2007 to 2019, she was a Staff Scientist with Lawrence Berkeley National Laboratory, Berkeley, CA, USA. In 2019, she joined the Faculty of Rice University, Houston, TX, USA, as a Professor of

biosciences with a joint appointment in bioengineering. Her research interests include exploring the interface between living organisms and non-living materials, and engineering this interface for applications in energy, environment, and biomedicine. She was the recipient of the Women@ the Lab Award in 2018, and as the Cancer Prevention and Research Institute of Texas Scholar in 2019. She is on the Editorial Board of the ACS Synthetic Biology and is the Editor of the mSystems.



Hua Wang (Senior Member, IEEE) received the M.S. and Ph.D. degrees in electrical engineering from the California Institute of Technology, Pasadena, CA, USA, in 2007 and 2009, respectively. He was with Intel Corporation and Skyworks Solutions. In 2012, he joined the School of Electrical and Computer Engineering, Georgia Institute of Technology, Atlanta, GA, USA, where he is currently an Associate Professor. He is the Director of Georgia Tech Center of Circuits and Systems, and the Director of the Georgia Tech Electronics and Micro-System lab. He

has authored or coauthored more than 190 peer-reviewed journal and conference papers. His interests include innovating analog, mixed-signal, RF, and mm-Wave integrated circuits and hybrid systems for wireless communication, sensing, and bioelectronics applications. He was the recipient of DARPA Director's Fellowship Award in 2020, DARPA Young Faculty Award in 2018, National Science Foundation CAREER Award in 2015, Qualcomm Faculty Award 2020, IEEE MTT-S Outstanding Young Engineer Award in 2017, Georgia Tech Sigma Xi Young Faculty Award in 2016, Georgia Tech ECE Outstanding Junior Faculty Member Award in 2015, and Lockheed Dean's Excellence in Teaching Award in 2015. From 2014 to 2018, he held the Demetrius T. Paris Professorship. His GEMS research group was the recipient of multiple Academic awards and best paper awards, including 2019 Marconi Society Paul Baran Young Scholar, IEEE RFIC Best Student Paper Award (1st Place in 2014, 2nd Place in 2016, and 2nd Place in 2018), IEEE CICC Outstanding Student Paper Award in 2015, 2018, and 2019, IEEE CICC Best Conference Paper Award in 2017, 2016 IEEE Microwave Magazine Best Paper Award, and IEEE SENSORS Best Live Demo Award, 2nd Place in 2016. He is a Technical Program Committee Member of IEEE ISSCC, RFIC, CICC, and BCICTS conferences. He is a Steering Committee Member of the IEEE, RFIC, and CICC. He is the Conference Chair of CICC 2019 and Conference General Chair of CICC 2020. He is a Distinguished Lecturer of IEEE Solid-State Circuits Society (SSCS) for the term of 2018–2019. He is the Chair of Atlanta's IEEE CAS/SSCS joint chapter that won IEEE SSCS Outstanding Chapter Award in 2014.